Interface originated modification of electron-vibration coupling in resonant photoelectron spectroscopy

C. Sauer, M. Wießner, A. Schöll,* and F. Reinert

Universität Würzburg, Experimentelle Physik VII & Röntgen Research Center for Complex Material Systems RCCM, 97074 Würzburg, Germany and Karlsruher Institut für Technologie KIT, Gemeinschaftslabor für Nanoanalytik, 76021 Karlsruhe, Germany

(Received 5 November 2013; revised manuscript received 23 January 2014; published 12 February 2014)

We present a comprehensive study of the photon-energy ($h\nu$)-dependent line-shape evolution of molecular orbital signals of large π-conjugated molecules by resonant photoelectron spectroscopy (RPES). A comparison to RPES data on small molecules suggests that the excitation into different vibrational levels on the intermediate-state potential energy surface of the electronic excitation is responsible for the observed effect. In this simplified picture of electron-vibration coupling the character of the potential energy surfaces involved in the RPES process determines the line shape of the molecular orbital signal for a particular $h\nu$. We use the sensitivity of this effect to probe the influence of different interfaces on the electron-vibration coupling in the investigated systems. The magnitude of the variation in line shape throughout the particular $h\nu$ region allows us to reveal significant differences within the physisorptive regime.

DOI: 10.1103/PhysRevB.89.075413 PACS number(s): 73.20.Hb, 79.60.Jv, 79.60.Fr, 68.35.Ja

I. INTRODUCTION

A generally interesting aspect in the description of quantum mechanical systems is the coupling of different excitations to one another. A prominent example is electron-vibration coupling, i.e., the excitation of vibrations accompanied to electronic excitations. Within the Born-Oppenheimer approximation and by the Franck-Condon principle, a fairly simple and intuitive picture of electron-vibration coupling in photoelectron spectroscopy (PES) [1] and near-edge x-ray absorption fine-structure (NEXAFS) spectroscopy [2] is achieved. This allows us to obtain information about electron-vibration coupling by analyzing the line shape of PES spectra of large π-conjugated molecules and thereby extracting a crucial parameter for charge transfer [3,4] in application relevant systems [5]. With a line-shape analysis of NEXAFS spectra of such molecules, parameters of the core excited potential energy surface can be obtained [6]. In special cases an electron-vibration coupling investigation of NEXAFS line shapes can even serve as a probe for electronic coupling of molecules [7]. Due to the surface sensitivity of PES and partial electron yield NEXAFS these techniques are well suited for study of thin films and interfaces. Furthermore, NEXAFS excitations at different elements or different chemical species of the same element can provide site-specific information for homomolecular systems. For heteromolecular systems [8–13] the excitation can be chosen to obtain molecule specific information.

Resonant PES (RPES) allows us to take the investigation of electron-vibration coupling to a next level. RPES experiments on small molecules (CO, N_2, O_2) in the gas phase in comparison to calculations, for example, reveal that lifetime vibrational interference [14,15] or $h\nu$ detuning [16] can significantly alter the line shape of molecular orbital derived signals, which is determined by the electron-vibration coupling. Using state-of-the-art experimental equipment in combination with theoretical analysis, even imaging of the ionic molecular potentials and mapping of vibrational wave functions are feasible for a simple molecule such as N_2 [17].

A comparable RPES investigation of the intensively studied large π-conjugated molecules leads to a dramatic increase in complexity. The many close-lying electronic excitations in the NEXAFS spectrum and the possibility of multiple vibronic modes coupling to each of them and to each other pose a tremendous challenge for an investigation of electron-vibration coupling. However, the application of this powerful technique to such complicated systems not only raises the level of complexity but also, in fact, allows us to obtain additional information with respect to PES or NEXAFS alone, while simultaneously retaining the advantages of both. A selective excitation into highly excited vibrational levels ν_i in the intermediate state leads to a line shape of the RPES signal from molecular orbitals which is very sensitive to the character of the involved potential energy surfaces V (ground state V_g, intermediate state V_i, and final state V_f). Thus, in principle, RPES is able to investigate electron-vibration coupling in the final as well as in the core excited intermediate state if the line shape of a proper signal can be analyzed in sufficient detail.

In this work we want to push the investigation of electron-vibration coupling in large π-conjugated molecules forward by performing a large comprehensive study on the $h\nu$-dependent evolution of the line shape of molecular orbital signals in RPES. This previously observed effect [18,19] is first discussed for the signal originating from the highest occupied molecular orbital (HOMO) of a copper-phthalocyanine (CuPc) multilayer and then related to RPES investigations of small molecules. This comparison is used to develop a simplified picture in which the character of the involved potential energy surfaces are the only parameters necessary to consistently discuss the observed line-shape evolutions. Both the discontinuous line-shape evolution of coronene and the continuous line-shape evolution of CuPc and tin-phthalocyanine (SnPc) in the energy region of interest are related to examples of small molecules. The parallel but NEXAFS resonance-specific behavior of the signals from the three frontier molecular orbitals of coronene constitutes an additional successful consistency check of the applied picture. Moreover, the sensitivity of the technique is

*achim.schoell@physik.uni-wuerzburg.de

revealed by a comparison of CuPc and SnPc multilayer films and then used to probe the influence of different interfaces. It is found that the adsorption on Au(111) influences the line-shape evolution of the HOMO signal of CuPc and SnPc differently in contrast to the similar modification observed at a hetero-organic interface. In the former case less relative intensity in high-final-state vibrational levels ν_f with respect to the multilayer is observed for CuPc on Au(111), while SnPc exhibits no significant alteration. In the latter case both systems show an interface-induced enhancement of relative intensity distribution into higher ν_f. Finally, we present a resonance-specific interface modification of the $h\nu$-dependent line-shape evolution by the adsorption of coronene on Ag(111). All observed changes can be consistently discussed on the basis of an influence on the character of the potential energy surfaces involved in the RPES process.

II. EXPERIMENTAL

RPES measurements were performed at BESSY II at the undulator beam line UE52-PGM ($E/\Delta E > 14000$ at 400 eV photon energy, with cff = 10 and a 20-μm exit slit [20]) in a UHV chamber with a pressure below 5×10^{-10} mbar. All PES maps were recorded with p-polarized light at a 70° angle of incidence with respect to the surface normal, a beam-line exit slit of 40 μm, and a cff value of 10. This results in an $h\nu$ resolution of better than 40 meV at 290 eV. Photoelectron intensities were measured with a Scienta R4000 electron analyzer, which was operated in transmission mode with an entrance slit of 300 μm. For the PES overview maps [see Figs. 1(a) and 2(a)] a pass energy of 100 eV, and for the PES detail maps [see Figs. 1(c) and 2(c)] and all one-dimensional (1D) energy distribution curve (EDC) waterfall plots a pass energy of 50 eV, was used, resulting

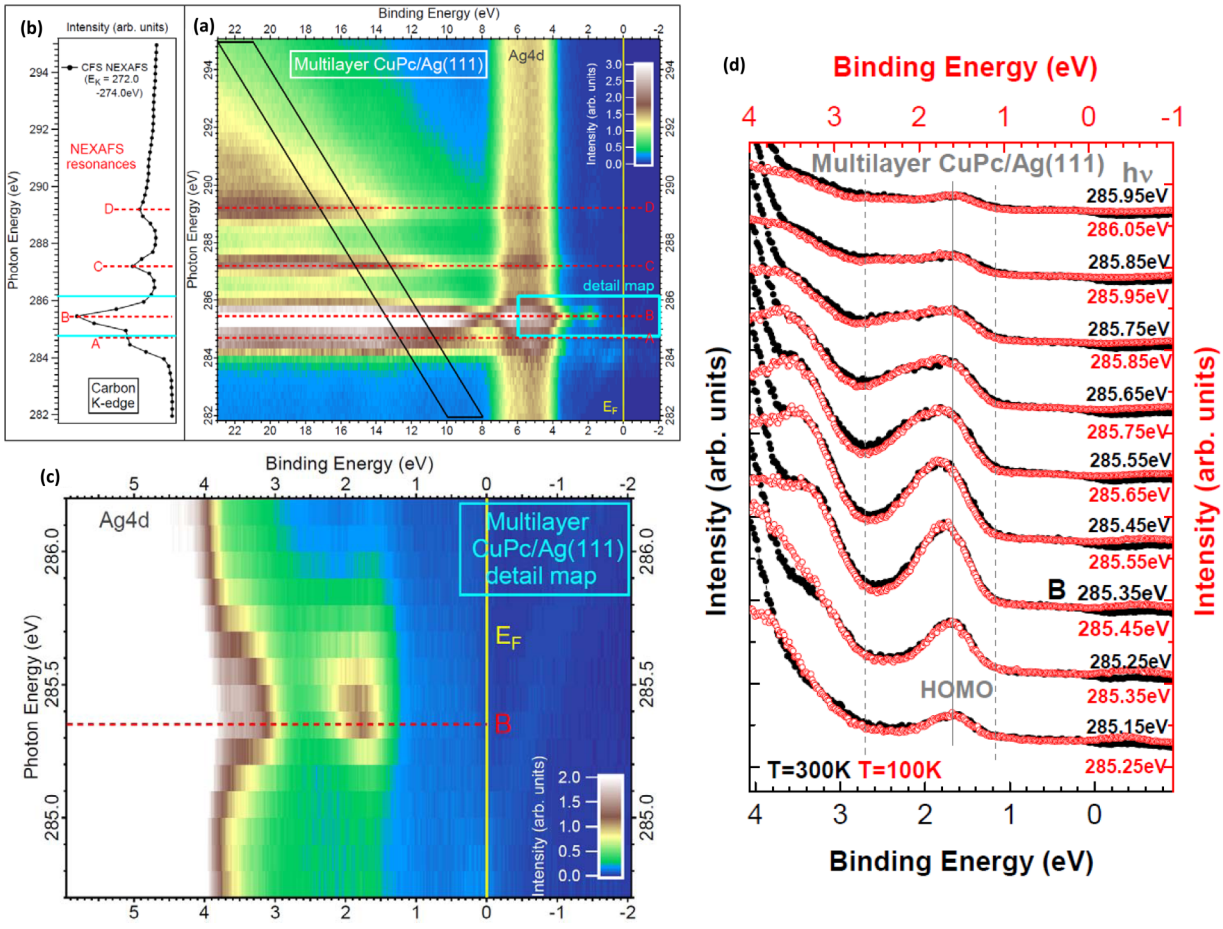

FIG. 1. (Color online) Full RPES data set of a multilayer CuPc/Ag(111) sample recorded at the carbon K edge. The PES maps are normalized according to the procedure given in the text. (a) PES overview map with an $h\nu$ increment of 250 meV and an E_B increment of 50 meV. (b) CFS NEXAFS extracted from the black parallelogram in the PES overview map (for details see text). Cyan lines denote the region probed by the PES detail map. (c) PES detail map with an $h\nu$ increment of 100 meV and an E_B increment of 15 meV. The feature around 0 eV E_B at the bottom of the PES map, which disperses to a lower E_B with increasing $h\nu$, is the the second-order C1s signal. (d) EDCs from the PES detail map (filled black circles) presented in a waterfall plot in comparison to corresponding EDCs from a PES detail map of a multilayer CuPc/Ag(111) sample prepared and measured at $T = 100$ K [open (red) circles]. EDCs of equivalent $h\nu$ positions within resonance B (resonance maximum denoted by the larger $h\nu$) are compared to each other (for details see text). Black axes (E_B and intensity) correspond to black EDCs, and red axes to red EDCs. The red E_B axis is shifted by -70 meV with respect to the black one. The intensities of the $T = 300$ K EDCs are unchanged, while for each of the $T = 100$ K EDCs an offset was added for a matching prepeak plateau (differently damped substrate signal) and a scaling factor for best comparability of the line shape of the HOMO signal was applied.

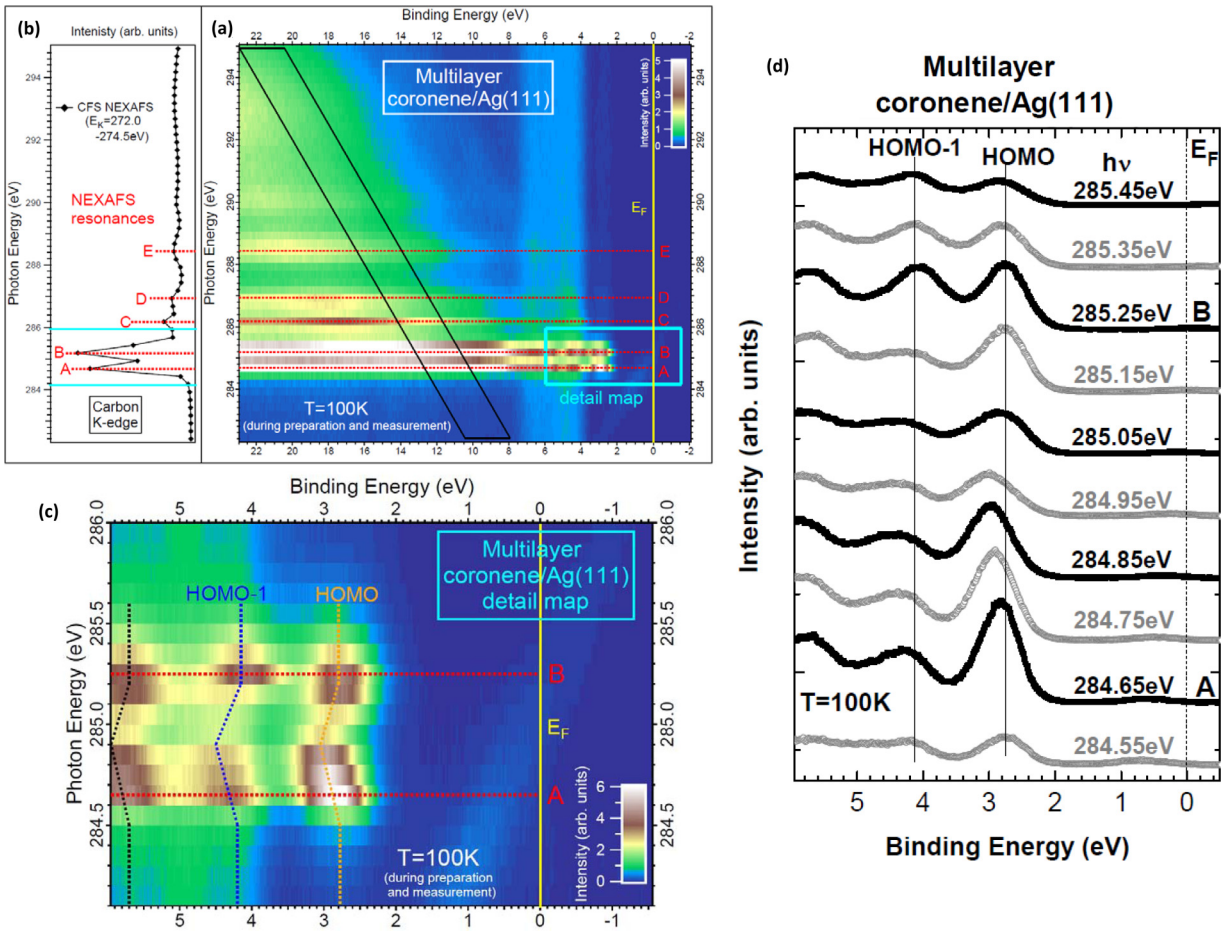

FIG. 2. (Color online) Full carbon K-edge RPES data set of a multilayer coronene/Ag(111) sample prepared and measured at $T = 100$ K. The PES maps are normalized according to the procedure given in the text. (a) PES overview map with an $h\nu$ increment of 250 meV and an E_B increment of 50 meV. (b) CFS NEXAFS extracted from the black parallelogram in the PES overview map (for details see text). Cyan lines denote the region of the PES detail map. (c) PES detail map with an $h\nu$ increment of 100 meV and an E_B increment of 15 meV. Dotted vertical lines are a guide for the eye and represent the roughly parallel evolution of the MO peak maxima. The feature around 1 eV E_B at the bottom of the PES map, which disperses to a lower E_B with increasing $h\nu$, is the the second-order C1s signal. (d) EDCs from the PES detail map presented in a waterfall plot.

in an energy resolution of $\Delta E = 150$ meV for the former and $\Delta E = 75$ meV for the latter. $h\nu$ was calibrated with the Fermi edge (E_F) after the measurement of a PES map and the binding energy ($E_B = h\nu - E_K$) and $h\nu$ of the EDCs were shifted rigidly by the obtained offset. The resulting accuracy of both energy scales is better than $\Delta h\nu = \Delta E_B = 50$ meV. Intensities were normalized to the ring current and the beamline flux curve, which was recorded separately by measuring the $h\nu$ dependence of the intensity of a PES signal of the clean surface.

The Ag(111) and Au(111) substrates were cleaned by several sputter and annealing cycles and their cleanness was confirmed by PES. All molecules were previously purified by sublimation and evaporated from Knudsen cells at pressures below 10^{-8} mbar and with the substrate kept at 300 K (unless denoted differently). The hetero-organic film was prepared by, first, depositing a multilayer of 3,4,9,10-perylene-tetracarboxylic-dianhydride (PTCDA); second, tempering the film at 300°C, which results in a single monolayer (ML) of PTCDA; and, finally, depositing a submonolayer of CuPc. After each preparation step the sample was checked by PES measurements. Film thicknesses were determined by core level intensities of the uppermost layers, damping factors of underlying core level signals using the effective electron attenuation lengths given in Ref. [21], and the emergence of multilayer originated features. The samples were carefully checked for radiation damage after RPES data acquisition.

III. RESULTS AND DISCUSSION

In order to identify proper molecular orbital signals for an $h\nu$-dependent line-shape investigation our first step is to record a PES overview map [see Figs. 1(a) and 2(a)], with the E_B ranging from approximately -2 to 23 eV and $h\nu$ including the intense π resonances. In the resulting PES overview map we are then able to select the area in which the PES detail map [see Figs. 1(c) and 2(c)] is recorded in a subsequent measurement with smaller increments (see figure captions) for both $h\nu$ and E_B. While the $h\nu$-dependent E_B dispersion is more obvious in the 2D PES detail map, a line-shape evolution can be observed better in a waterfall plot of 1D EDCs, especially when signals vary strongly in intensity. Thus for the general

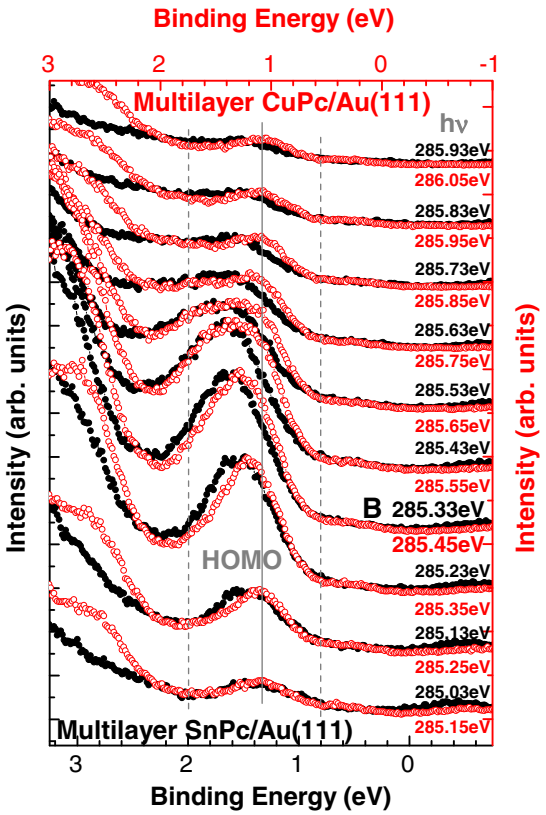

FIG. 3. (Color online) Waterfall plot of EDCs from a multilayer CuPc/Au(111) [open (red) circles] compared to EDCs from a multilayer of SnPc/Au(111) (filled black circles). EDCs of equivalent $h\nu$ positions within the resonance (resonance maximum denoted by the larger $h\nu$) are compared to each other (for details see text). Black axes (E_B and intensity) correspond to black EDCs, and red axes to lighter (red) EDCs. The lighter (red) E_B axis was shifted by −250 meV with respect to the black one. PES detail maps from which the EDCs originate were normalized according to the procedure given in the text. The intensities of the SnPc EDCs are unchanged, while each of the CuPc EDCs is scaled for best comparability of the line shape of the HOMO signal.

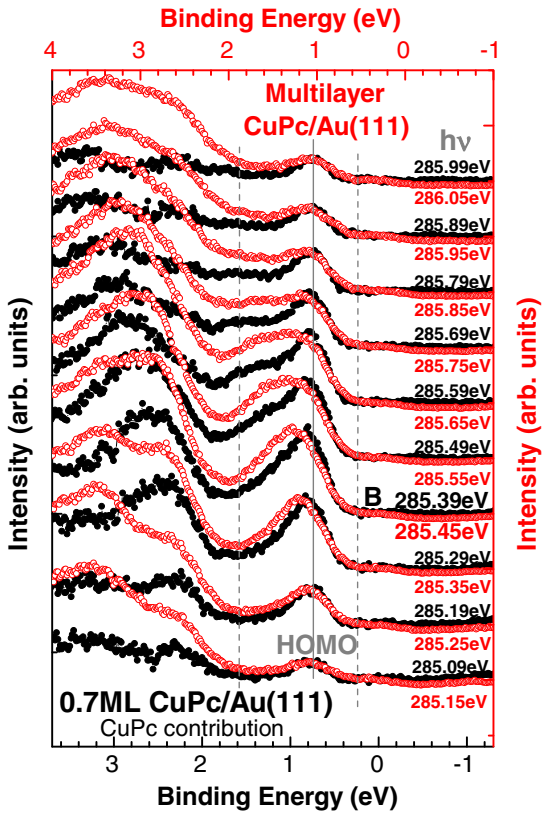

FIG. 4. (Color online) Waterfall plot of EDCs from a multilayer CuPc/Au(111) [open (red) circles] compared to EDCs from a 0.7-ML CuPc/Au(111) (filled black circles). EDCs of equivalent $h\nu$ positions within the resonance (resonance maximum denoted by the larger $h\nu$) are compared to each other (for details see text). Black axes (E_B and intensity) correspond to black EDCs, and lighter (red) axes to red EDCs. The red E_B axis is shifted by 300 meV with respect to the black one. PES detail maps from which the EDCs originate are normalized according to the procedure given in the text. For the 0.7-ML CuPc/Au(111) EDCs the scaled Au(111) substrate EDCs at equal $h\nu$ are subtracted and the intensities are unchanged. To each of the multilayer CuPc EDCs an offset is added for a matching prepeak plateau [clean Au(111) subtracted only for the 0.7-ML CuPc EDCs] and a scaling factor for best comparability of the line shape of the HOMO signal is applied.

discussion of the $h\nu$-dependent line-shape evolution (Figs. 1 and 2) we present the detailed RPES data in both ways and restrict the data presentation to EDC waterfall plots for the following comparison of different systems (Figs. 3–6).

A. The photoelectron spectroscopy map

In the present study RPES is always performed at the carbon K edge and the C1s electrons are excited into delocalized molecular orbitals of mainly π character. On-resonance PES signals stemming from the adsorbed organic molecules are massively enhanced with respect to substrate PES signals. The states produced in the RPES process are one-hole final states along with additional two-hole final states, which can further be divided into those with an additional electron in an excited state and those without. Above ionization threshold this electron cannot be present since it has been excited into vacuum. In the PES overview map [Figs. 1(a) and 2(a)] the features at high E_B (8–23 eV) consist of both two-hole final states and one-hole final states from lower-lying molecular orbitals. These are located at the same E_B as in an off-resonant (or direct) PES measurement. Integrating a constant E_K window [black parallelogram in Figs. 1(a) and 2(a)] in this energetic region results in the 1D spectrum presented in Figs. 1(b) and 2(b). This approach is called constant final-state (CFS) spectroscopy, while the integration over a constant E_B window is usually referred to as constant initial-state (CIS) spectroscopy. For the obtained $h\nu$ increment the CFS spectrum is equal to the particular traditional partial electron yield NEXAFS spectrum, while the CIS spectrum shows differences, especially for the larger-$h\nu$ region. This can be explained by the fact that above ionization threshold this region mainly consists of Auger signals, which remain at constant E_K with varying $h\nu$. The equivalence of this CFS NEXAFS spectrum and the partial electron yield NEXAFS means that for the assignment of the NEXAFS resonances the

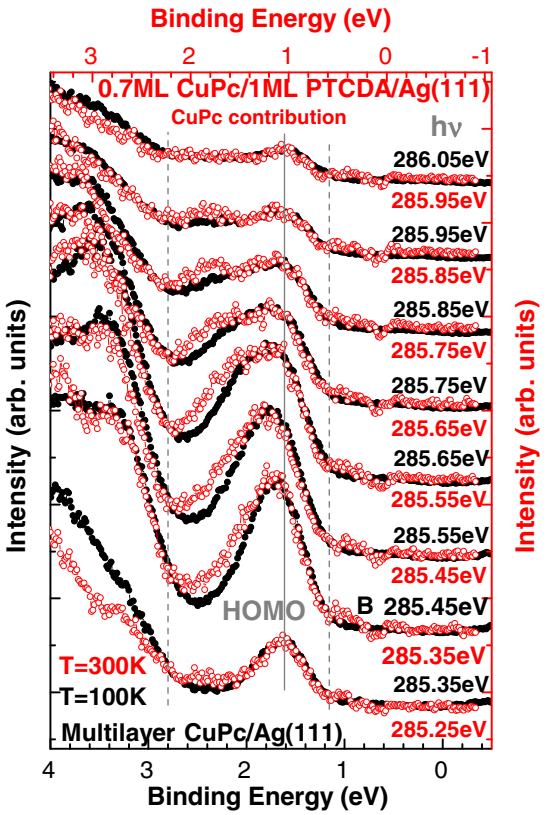

FIG. 5. (Color online) Waterfall plot of EDCs from a multilayer CuPc/Ag(111) prepared and measured at $T = 100$ K (filled black circles) compared to EDCs from a 0.7-ML CuPc/1-ML PTCDA/Ag(111) [open (red) circles]. EDCs of equivalent $h\nu$ positions within the resonance (resonance maximum denoted by the larger $h\nu$) are compared to each other (for details see text). Black axes (E_B and intensity) correspond to black EDCs, and lighter (red) axes to red EDCs. The red E_B axis is shifted by -570 meV with respect to the black one. PES detail maps from which the EDCs originate are normalized according to the procedure given in the text. For the 0.7-ML CuPc/1-ML PTCDA/Ag(111) EDCs, scaled 1-ML PTCDA/Ag(111) EDCs at an equal $h\nu$ (from Ref. [36]) are subtracted and each EDC is scaled for best comparability of the line shape of the HOMO signal.

PES overview map itself can be used. This has the advantage that a comparison of intensities to another signal in the PES map is independent of the normalization procedure, which might lead to delicate artifacts [22].

The signals of interest in this work are the one-hole final states, which are situated at lower E_B values (0–6 eV) in the PES overview map. In the investigated large π-conjugated molecules these states stemming from the frontier molecular orbitals (HOMO, etc.) are usually separated from each other in E_B. If the coupling to the surrounding is small they are also separated from all two-hole final-state features. In this case a final state with two holes in the HOMO is the lowest bound state possible and this state is situated at considerably larger E_B. Thus they are ideal candidates for an electron-vibration coupling investigation by an $h\nu$-dependent line-shape analysis. Unfortunately the situation is expected to be more complicated in the $h\nu$ direction. A variety of close-lying electronic transitions could contribute to the $h\nu$ region in which the separated signal from the molecular orbitals is intense enough for a significant line-shape analysis. Additionally, multiple vibrational modes could simultaneously couple to each of these electronic transitions and to each other, leading to an overlap of many contributions within a small $h\nu$ range. It turns out that this complicated situation can be overcome by a comparison to much simpler molecules. On the basis of this comparison to systems for which calculations are feasible the large RPES data set analyzed in this work can be discussed by including the character of the involved potential energy surfaces as the only parameters.

B. Photon-energy-dependent line-shape evolution of molecular orbital signals

In Fig. 1 the complete RPES data set of a multilayer CuPc/Ag(111) is presented. Figure 1(a) shows the PES overview map from which the CFS NEXAFS was extracted [integration of the black parallelogram in Fig. 1(a) leads to the spectrum in Fig. 1(b)] and used for the identification of NEXAFS resonances A–D. A pronounced increase in intensity of the HOMO signal is observed in resonance B so this part of the PES overview map (cyan box) is selected for closer inspection by a PES detail map [Fig. 1(c)]. Here the resonance maximum [dashed (red) line] is defined to be the EDC with the highest intensity at the E_B position of the HOMO signal in direct PES. Starting just before the resonance maximum the maximum of the HOMO signal continuously disperses to higher E_B with increasing $h\nu$. The EDC waterfall plot [Fig. 1(d)] allows us to identify this effect as a gradual redistribution of intensity towards higher E_B within the HOMO signal. This results in a line-shape evolution from symmetric to more and more asymmetric and, finally, to two separated peaks. The black EDCs, which originate from the PES detail map in Fig. 1(c), hereby evolve parallel to the lighter (red) EDCs, which stem from a corresponding PES detail map of a multilayer CuPc prepared and measured at $T = 100$ K. The EDCs are aligned at the same position within resonance B; i.e., both EDCs of the resonance maximum are compared to each other, and so on. Interestingly the EDCs of the 300 K sample, which grows in a Stranski-Krastanow mode, have to be shifted in $h\nu$ and E_B for comparison to the 100 K sample exhibiting layer-by-layer type growth. However, both samples show an identical line-shape evolution. An imprecise energy calibration can be excluded as a reason for the energy mismatch since the HOMO E_B positions exhibit the same shift in the corresponding off-resonant ($h\nu = 120$ eV) PES data. Apparently, the difference in growth mode influences the peak positions in (R)PES and NEXAFS but not the origin of the $h\nu$-dependent line-shape evolution. This is further confirmed by a comparison to the EDCs of a multilayer CuPc/Au(111), which exhibit the same line-shape evolution as the two systems displayed in Fig. 1(d).

Up to now a proper treatment of electronic interference effects in the RPES process [23,24] or lifetime vibrational interference [14,15] has not been feasible due to the complexity of the electronic and vibrational structure of the investigated large π-conjugated molecules. Not even the assignment of electronic transitions that contribute to the NEXAFS resonance

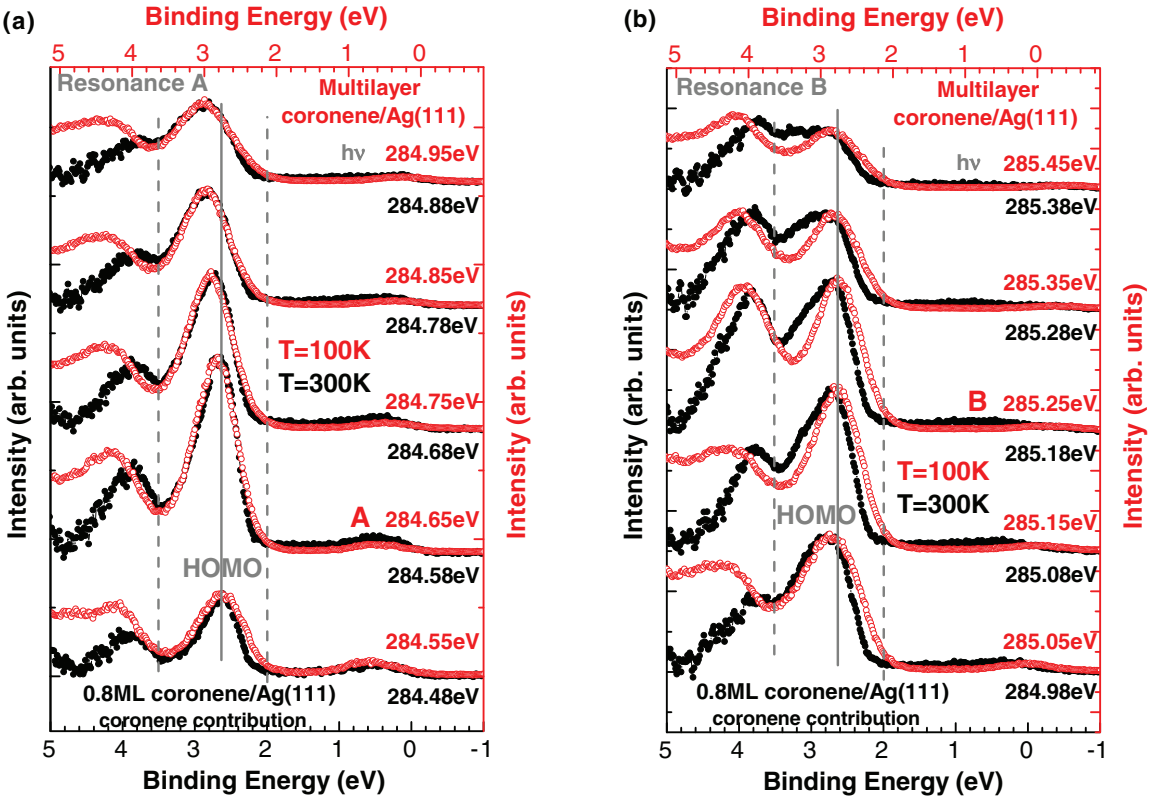

FIG. 6. (Color online) Waterfall plot of EDCs from a multilayer coronene/Ag(111) prepared and measured at $T = 100$ K [open (red) circles] compared to EDCs from an 0.8-ML coronene/Ag(111) (filled black circles). EDCs of equivalent $h\nu$ positions within the resonance (resonance maximum denoted by "A" and "B") are compared to each other (for details see text). Black axes (E_B and intensity) correspond to black EDCs, and lighter (red) axes to red EDCs. The red E_B axis is shifted by 130 meV with respect to the black one. PES detail maps from which the EDCs originate are normalized according to the procedure given in the text. For the 0.8-ML coronene/Ag(111) EDCs scaled Ag(111) substrate EDCs at equal $h\nu$ are subtracted and the intensities are unchanged. Each of the multilayer coronene EDCs is scaled for best comparability of the line shape of the HOMO signal. (a) $h\nu$ region of NEXAFS resonance A. (b) $h\nu$ region of NEXAFS resonance B.

B of CuPc is unambiguously determined in the literature [25–27]. Hence we cannot draw any conclusion from theoretical calculations performed on the system investigated here. Instead we compare the RPES data on CuPc to studies of smaller molecules for which RPES calculations are feasible. In several studies of small molecules [14,15,28,29] (CO, N_2, O_2, and OCS) a quite similar $h\nu$-dependent line-shape evolution of the molecular orbital signals (usually termed participator decays in these publications) is observed. The case of CO constitutes the simplest scenario of one electronic transition in the NEXAFS spectrum and one vibration coupling to it. Therefore the different vibronic peaks contributing to the molecular orbital signals can be resolved and a selective excitation into one particular vibrational level ($\nu_i = 0, 1, 2$) of the intermediate-state potential energy surface (V_i) in RPES is possible. In CO it is found that the higher the ν_i of the excitation into the V_i is, the more relative intensity is distributed into higher vibrational final-state levels ν_f of the molecular orbital signals. In a Franck-Condon picture this means that the character of the potential energy surfaces governs the relative intensities of the different ν_f contributions to the molecular orbital signal for a particular $h\nu$. Relative intensity changes between the ν_f peaks for EDCs recorded with different $h\nu$ values are thus the reason for the line-shape evolution. If the different ν_f peaks cannot be resolved, this electron-vibration coupling originated effect leads to a successively increasing relative intensity in the high-E_B part of the molecular orbital peak with increasing $h\nu$. This is exactly the observation seen for the CuPc HOMO signal in Fig. 1(d). So we conclude that this $h\nu$-dependent line-shape evolution can be discussed analogously to CO. Hence the excitation into different ν_i and the consequential characteristic distribution of the relative intensity (Franck-Condon factors) of the ν_f is the basis of the following discussion. Consequently the character of the potential energy surface in the ground state (V_g), in the intermediate state (V_i), and in the final state (V_f) are the parameters which determine the line-shape evolution in the picture we use to discuss the large π-conjugated molecules in this work. Furthermore, the observation of a continuous line-shape evolution in Fig. 1(d) points towards one dominating electronic contribution to the RPES in the $h\nu$ direction so that, despite its complicated electronic structure, CuPc can be compared to CO. Multiple electronic transitions with a small difference in $h\nu$ would also result in a continuous line-shape evolution and cannot be excluded. In this case we would have to speak of one effective electronic transition that is responsible for the observed HOMO signal in RPES in Fig. 1(d). However, the comparability to CO is reasonable in both cases.

We would like to note that in a previous discussion of the RPES data of SnPc the line-shape evolution of molecular

orbital signals was explained by $h\nu$ detuning from the contributing electronic transition in the NEXAFS spectrum [19]. Based on the present large data set we consider the above-described excitation into different ν_i the dominating effect for the observed line-shape changes within the investigated $h\nu$ regime.

For a multilayer coronene/Ag(111) a complete RPES data set is presented in Fig. 2 analogously to CuPc in Fig. 1. The PES detail map [Fig. 2(c)] and the EDC waterfall plot [Fig. 2(d)] of this system do not show the same overall continuous line-shape evolution as for CuPc. In coronene the HOMO peak maximum first disperses to a higher E_B with increasing $h\nu$ starting at the maximum of resonance A. Then, between resonance A and resonance B, it moves back to its original E_B position and remains almost unchanged with further increasing $h\nu$. This noncontinuous evolution scenario is quite similar to that for H_2CO [30] and NO [31]. In the former multiple simultaneously exited vibronic modes contribute to the NEXAFS spectrum with one electronic transition [32]. In the latter multiple electronic transitions are present in the NEXAFS spectrum, with the single vibrational mode of NO coupling to them [31]. Both scenarios are generally possible for the $h\nu$ region from 284.4 to 285.6 eV in the RPES data on coronene. NEXAFS calculations suggest that there is one electronic transition in resonance A and another two in resonance B [33] and the line shape of the high-resolution partial electron yield NEXAFS spectrum (not shown) corroborates this scenario of multiple electronic transitions. A significant contribution to the RPES from the single transition in resonance A is clearly observed. Hence for the $h\nu$ region around resonance A ($h\nu = 284.55$–284.95 eV) the HOMO signal line-shape evolution of coronene can be explained in the same way as for CuPc described above. Further data on a sample of multilayer coronene/Ag(111) prepared and measured at 300 K and recorded with a 50-meV $h\nu$ increment (not shown) confirm the continuous evolution observed for the HOMO signal around resonance A. Whether there is a contribution to the RPES from no, one, or two electronic transitions in NEXAFS resonance B cannot be concluded from the data. However, in any of these cases the intensity and line-shape evolution can be discussed analogously since, for a second electronic transition as well as a higher excited vibrational series of the first electronic transition, higher ν_i are excited by higher $h\nu$. The E_B dispersion of the HOMO peak between resonance A and resonance B is probably a consequence of the decreasing intensity at higher ν_i within NEXAFS resonance A and the simultaneous increase in the intensity at low ν_i within NEXAFS resonance B. So a peak with more relative intensity at higher E_B gradually transforms into a peak with more relative intensity at lower E_B. For the $h\nu$ region around resonance B ($h\nu = 285.15$–285.45 eV) a less pronounced redistribution of relative intensity to higher E_B with increasing $h\nu$ is found. In the Franck-Condon picture discussed above this is the consequence of a difference in the V_i. The fact that all three visible molecular orbital signals in Fig. 2(c) evolve in an almost-parallel way (see dotted vertical lines, which roughly represent the peak maximum) but different in resonances A and B further corroborates this conclusion. The observed resonance-specific line-shape evolution requires an explanation with a parameter determined by the excitation such as V_i. The parallel evolution then suggests similar V_f for the three molecular orbital signals, which is reasonable due to the π-dominated character of these frontier molecular orbitals.

The comparison of the $h\nu$-dependent line-shape evolution in RPES for CuPc and SnPc multilayers displayed in Fig. 3 serves as another consistency check for consideration of the character of the potential energy surfaces as the dominant parameters. Both molecules have a very similar overall electronic structure, and in particular a basically equal HOMO, because there is no contribution to it by the center metal atom [34,35]. Thus the geometric difference between the two molecules constitutes the most reasonable explanation for the observed difference visible in the HOMO signal line-shape evolution. A difference in electron-vibration coupling in the RPES process is not surprising for the bent SnPc with respect to the flat CuPc. Hence the character of the potential energy surfaces can also explain the origin of the difference between these two systems. The fact that both HOMO signal line shapes are almost equal at the lowest $h\nu$ in Fig. 3 but then evolve differently throughout the resonance reveals the sensitivity of the technique. Even in a moderate E_B resolution leading to symmetric and similar peaks for both molecules in direct PES a difference in the HOMO signal line-shape evolution is found. In the following section we explore the potential of this line-shape evolution in RPES as a probe for variations in the molecular environment.

C. Modification of the electron-vibration coupling by different interfaces

Comparing the line-shape evolution of a multilayer CuPc/Au(111) with a submonolayer CuPc/Au(111) in Fig. 4 exposes a clear difference between the two systems. As shown in Fig. 3 an equal line shape at the lowest $h\nu$ evolves differently at higher $h\nu$. In this example the difference can be characterized as less distribution of relative intensity into the higher E_B part of the HOMO signal for CuPc adsorbed on Au(111). In other words the excitation of higher ν_f in the RPES process is somewhat prohibited. Such an influence due to the adsorption on a metal surface on the character of the involved potential energy surfaces is reasonable and thus fits into the overall discussion. A comparison of electron-vibration coupling in direct PES of submonolayer or ML samples with respect to multilayer films is usually hindered by broadening due to disorder in the multilayer. In RPES the involvement of an additional V_i and the possibility of exciting high ν_i in this V_i results in changes in the line shape beyond the broadening due to disorder. So for the molecules investigated here the $h\nu$-dependent line-shape evolution of molecular orbital signals in RPES allows us to identify interface originated modifications of electron-vibration coupling. Additionally, both systems compared in Fig. 4 are usually characterized as weakly interacting because there is no significant electronic interaction that manifests itself in strongly altered PES spectra of the adsorbed molecule with respect to the multilayer film. The revelation of differences within this so-called physisorptive regime further indicates the sensitivity of the effect. Remarkably, the analogous comparison of a submonolayer SnPc/Au(111) with a multilayer SnPc/Au(111) (not shown) exhibits a parallel $h\nu$-dependent line-shape evolution of the

SnPc HOMO signal. Hence the potential energy surfaces of SnPc are not significantly altered by the adsorption on Au(111). Consequently not only does the electron-vibration coupling of the bent SnPc molecule differ from that of the flat CuPc, but also a difference in the influence of the Au(111) surface on the electron-vibration coupling in both molecules is observed.

By depositing a submonolayer or ML of SnPc [11,12] or CuPc [13] onto 1-ML PTCDA/Ag(111) a stable and vertically well-defined interface can be prepared. The comparison of the $h\nu$-dependent line-shape evolution of the CuPc HOMO signal of this hetero-organic system with a multilayer of CuPc/Ag(111) is displayed in Fig. 5. In contrast to the adsorption on Au(111) the excitation of higher ν_f in the RPES process is enhanced at this interface with respect to the multilayer film. For the SnPc/1-ML PTCDA/Ag(111) heteromolecular interface the same variation is found with respect to the SnPc multilayer [19]. The smaller $h\nu$ increment of the data presented here makes a clear identification of a continuous evolution possible and therefore shows that both SnPc and CuPc in the heteromolecular system can be discussed in the same way as for all other systems in this work. The similar change in both molecules in the heteromolecular system with respect to a multilayer sample becomes particularly interesting considering the fact that the reaction on the adsorption on Au(111) is different. We would like to note that additional RPES data on several systems with strong interfacial bonding and ground-state charge transfer into the molecule [1-ML PTCDA/Ag(110), 1-ML 1,4,5,8-naphthalene-tetracarboxylic dianhydride/Ag(111), and 1-ML CuPc/Ag(111)] show very strong and characteristic line-shape changes with respect to the corresponding multilayer sample and have to be described within a different model. Hence in terms of interface modifications of electron-vibration coupling observed in RPES both SnPc and CuPc on PTCDA/Ag(111) must be considered weakly interacting, which is in contrast to another conclusion in the literature [13]. A detailed investigation of RPES applied to the strongly interacting systems mentioned above will be reported in a future publication.

For a multilayer of coronene a different line-shape evolution in RPES is found for the NEXAFS resonances A and B (see Fig. 2). This discussed difference in the character of the particular V_i also manifests itself in the reaction on the adsorption on a Ag(111) surface. A comparison of the submonolayer film on Ag(111) to the multilayer sample is displayed in Fig. 6. The $h\nu$ region around resonance A [Fig. 6(a)] shows a parallel line-shape evolution starting with the resonance maximum, while for the EDCs at the lowest $h\nu$ a broader HOMO signal is observed for the multilayer. This difference can be explained by increased inhomogeneity in the multilayer film. However, this effect becomes negligible as soon as the electron-vibration coupling originated line-shape evolution alters the HOMO signal to a much larger extent. In the $h\nu$ region around resonance B [Fig. 6(b)] the submonolayer sample EDCs exhibit more intensity in the high-E_B part of the HOMO peak than the multilayer EDCs. Thus the Ag(111) surface modifies the V_i such that the excitation of higher ν_f in the RPES process is enhanced with respect to the multilayer. A comparison of the line-shape evolution of two coronene multilayers prepared and measured at 100 and at 300 K (not shown) further corroborates the assignment of the difference in Fig. 6(b) as an interface effect. The difference in growth modes (300 K grows in a Stranski-Krastanow mode; 100 K, more in a layer-by-layer mode) has no significant influence on the line-shape evolution, analogous to the finding in CuPc discussed above. Consequently the example of a submonolayer of coronene/Ag(111) shown in Fig. 6 reveals that the interface originated modification of the electron-vibration coupling in RPES can even be characteristic for different NEXAFS resonances in the same system. This, once again, points towards a change in the V_i as the most reasonable origin for the observed differences in the $h\nu$-dependent line-shape evolution since these are resonance specific.

IV. SUMMARY AND CONCLUSION

In summary we present a comprehensive RPES study of several large π-conjugated molecules in multilayer films and at different interfaces. By the comparison to RPES investigations of small molecules we are able to discuss the observed $h\nu$-dependent line-shape evolution of molecular orbital signals within a picture based on electron-vibration coupling. The relative intensity distribution among excitations of vibrations in the final state for a particular $h\nu$ is suggested as the origin of the observed line-shape evolution. Within this simplified picture all systems and the differences between them are consistently discussed by the character of the potential energy surfaces involved in the RPES process. Consequently the influence of the particular interface on the mechanism of the excitation of these vibrations is given as the origin for changes with respect to the multilayer sample. We show that, depending on the specific interface, the relative intensity distributed into high vibrational levels in the final state can remain unchanged, be partially quenched, or be enhanced. On Au(111) the excitation of high vibrational levels is partially quenched for CuPc, while no influence is found for SnPc. Opposite to that, an enhancement of the high vibrational levels occurs at the hetero-organic interface of SnPc and CuPc on top of 1-ML PTCDA/Ag(111). With the adsorption of coronene on Ag(111) we present an example for a resonance-specific modification of electron-vibration coupling. In comparison to the multilayer film an enhancement of the contribution of high vibrations to the HOMO signal is demonstrated in only one of the two NEXAFS resonances.

This work illustrates the potential of line-shape investigations of molecular orbital signals in RPES as a sensitive probe for electron-vibration coupling in large π-conjugated molecules. By the presented magnitude of the $h\nu$-dependent variation inhomogeneous broadening and moderate energy resolution can be overcome, which allows us to reveal effects that are not visible in direct PES and NEXAFS spectroscopy alone. Therefore a smaller influence of an interface on electron-vibration coupling can be investigated by RPES with an equally high surface sensitivity. The fact that all the interface originated modifications found constitute differences within the physisorptive regime further demonstrates the sensitivity of the applied technique.

A detailed investigation of the specific character of the potential energy surfaces involved in RPES, like the role of

coupling between multiple vibronic modes and lifetime vibrational interference, can only be studied by direct comparison of our data with calculations. These are, to our best knowledge, not feasible for the investigated systems at this point. The same applies for electronic interference effects or a possible insufficiency of the Born-Oppenheimer approximation. We would like to stress that the importance of these effects cannot be excluded on the basis of this experimental work. However, the discussion given based on the comparison to small molecules draws a consistent picture for a large data set using the character of the potential energy surfaces as the only required parameters. With this work we hope to stimulate a significant advance in the theoretical treatment of RPES applied to the systems presented here, which is necessary to elevate the understanding of this technique to the next level.

ACKNOWLEDGMENTS

We thank the BESSY staff, F. Bruckner, S. Gusenleitner, and M. Scholz, for support during beam times. Further, we would like to thank F. Meyer for stimulating discussions about RPES in comparison to RIXS. This work was supported by BESSY, by the Bundesministerium für Bildung und Forschung (BMBF; Grant Nos. 05K10WW2 and 03SF0356B), and by the Deutsche Forschungsgemeinschaft (DFG; Grant Nos. GRK 1221 and RE1469/9-1).

[1] S. Hüfner, *Photoelectron Spectroscopy—Principles and Applications* (Springer-Verlag, Berlin, 1996).
[2] J. Stöhr, *NEXAFS Spectroscopy* (Springer-Verlag, Berlin, 1992).
[3] N. Ueno and S. Kera, Prog. Surf. Sci. **83**, 490 (2008).
[4] S. Kera, H. Yamane, and N. Ueno, Prog. Surf. Sci. **84**, 135 (2009).
[5] J. Hwang, A. Wan, and A. Kahn, Mater. Sci. Eng. R **64**, 1 (2009).
[6] A. Schöll, Y. Zou, L. Kilian, D. Hübner, D. Gador, C. Jung, S. G. Urquhart, T. Schmidt, R. Fink, and E. Umbach, Phys. Rev. Lett. **93**, 146406 (2004).
[7] M. Scholz, F. Holch, C. Sauer, M. Wiessner, A. Schöll, and F. Reinert, Phys. Rev. Lett. **111**, 048102 (2013).
[8] C. Bobisch, T. Wagner, A. Bannani, and R. Möller, J. Chem. Phys. **119**, 9804 (2003).
[9] W. Chen, H. Huang, S. Chen, L. Chen, H. L. Zhang, X. Y. Gao, and A. T. S. Wee, Appl. Phys. Lett. **91**, 114102 (2007).
[10] D. Kasemann, C. Wagner, R. Forker, T. Dienel, K. Müllen, and T. Fritz, Langmuir **25**, 12569 (2009).
[11] M. Häming, M. Greif, C. Sauer, A. Schöll, and F. Reinert, Phys. Rev. B **82**, 235432 (2010).
[12] M. Häming, M. Greif, M. Wießner, A. Schöll, and F. Reinert, Surf. Sci. **604**, 1619 (2010).
[13] B. Stadtmüller, T. Sueyoshi, G. Kichin, I. Kröger, S. Soubatch, R. Temirov, F. S. Tautz, and C. Kumpf, Phys. Rev. Lett. **108**, 106103 (2012).
[14] M. Neeb, J.-E. Rubensson, M. Biermann, and W. Eberhardt, J. Electron Spectrosc. Relat. Phenom. **67**, 261 (1994).
[15] S. Osborne, A. Ausmees, S. Svensson, A. Kivimäki, O. Sairanen, A. N. de Brito, H. Aksela, and S. Aksela, J. Chem. Phys. **102**, 7317 (1995).
[16] S. Sundin, F. Kh. Gel'mukhanov, H. Ågren, S. J. Osborne, A. Kikas, O. Björneholm, A. Ausmees, and S. Svensson, Phys. Rev. Lett. **79**, 1451 (1997).
[17] V. Kimberg, A. Lindblad, J. Söderström, O. Travnikova, C. Nicolas, Y. P. Sun, F. Gel'mukhanov, N. Kosugi, and C. Miron, Phys. Rev. X **3**, 011017 (2013).
[18] L. Kjeldgaard, T. Kääambre, J. Schiessling, I. Marenne, J. N. O'Shea, J. Schnadt, C. J. Glover, M. Nagasono, D. Nordlund, M. G. Garnier, L. Qian, J.-E. Rubensson, P. Rudolf, N. Mårtensson, J. Nordgren, and P. A. Brühwiler, Phys. Rev. B **72**, 205414 (2005).
[19] M. Häming, L. Weinhardt, A. Schöll, and F. Reinert, Chem. Phys. Lett. **510**, 82 (2011).
[20] M. L. M. Rocco, M. Haeming, D. R. Batchelor, R. Fink, A. Schöll, and E. Umbach, J. Chem. Phys. **129**, 074702 (2008).
[21] T. Graber, F. Forster, A. Schöll, and F. Reinert, Surf. Sci. **605**, 878 (2011).
[22] A. Schöll, Y. Zou, T. Schmidt, R. Fink, and E. Umbach, J. Electron Spectrosc. Relat. Phenom. **129**, 1 (2003).
[23] U. Fano, Phys. Rev. **124**, 1866 (1961).
[24] L. C. Davis and L. A. Feldkamp, Phys. Rev. B **23**, 6239 (1981).
[25] F. Evangelista, V. Carravetta, G. Stefani, B. Jansik, M. Alagia, S. Stranges, and A. Ruocco, J. Chem. Phys. **126**, 124709 (2007).
[26] M. Linares, S. Stafström, Z. Rinkevicius, H. Ågren, and P. Norman, J. Phys. Chem. B **115**, 5096 (2011).
[27] R. De Francesco, M. Stener, and G. Fronzoni, J. Phys. Chem. A **116**, 2885 (2012).
[28] M. N. Piancastelli, M. Neeb, A. Kivimäki, B. Kempgens, H. M. Köppe, K. Maier, A. M. Bradshaw, and R. F. Fink, J. Phys. B **30**, 5677 (1997).
[29] O. Travnikova, C. Miron, M. Bässler, R. Feifel, M. Piancastelli, S. Sorensen, and S. Svensson, J. Electron Spectrosc. Relat. Phenom. **174**, 100 (2009).
[30] J. Bozek, S. Canton, E. Kukk, and N. Berrah, Chem. Phys. **289**, 149 (2003).
[31] E. Kukk, G. Snell, J. D. Bozek, W.-T. Cheng, and N. Berrah, Phys. Rev. A **63**, 062702 (2001).
[32] G. Remmers, M. Domke, A. Puschmann, T. Mandel, C. Xue, G. Kaindl, E. Hudson, and D. A. Shirley, Phys. Rev. A **46**, 3935 (1992).
[33] H. Oji, R. Mitsumoto, E. Ito, H. Ishii, Y. Ouchi, K. Seki, T. Yokoyama, T. Ohta, and N. Kosugi, J. Chem. Phys. **109**, 10409 (1998).
[34] V. Y. Aristov, O. V. Molodtsova, V. V. Maslyuk, D. V. Vyalikh, V. M. Zhilin, Y. A. Ossipyan, T. Bredow, I. Mertig, and M. Knupfer, J. Chem. Phys. **128**, 034703 (2008).
[35] C. Stadler, S. Hansen, I. Kröger, C. Kumpf, and E. Umbach, Nat. Phys. **5**, 153 (2009).
[36] J. Ziroff, A. Schöll and F. Reinert, unpublished (2011).